Available online at www.sciencedirect.com

ScienceDirect

Geochimica et Cosmochimica Acta 192 (2016) 135–148

Geochimica et Cosmochimica Acta

www.elsevier.com/locate/gca

Cooling rates of LL, L and H chondrites and constraints on the duration of peak thermal conditions: Diffusion kinetic modeling and implications for fragmentation of asteroids and impact resetting of petrologic types

Jibamitra Ganguly [a,*], Massimiliano Tirone [b], Kenneth Domanik [c]

[a] Department of Geosciences, University of Arizona, Tucson, AZ 85721, USA
[b] Institut für Geologie, Mineralogie, Geophysik, Rühr-Universität, D-44780 Bochum, Germany
[c] Lunar and Planetary Laboratory, University of Arizona, Tucson, AZ 85721, USA

Received 12 October 2015; accepted in revised form 23 July 2016; Available online 2 August 2016

Abstract

We have carried out detailed thermometric and cooling history studies of several LL-, L- and H-chondrites of petrologic types 5 and 6. Among the selected samples, the low-temperature cooling of St. Séverin (LL6) has been constrained in an earlier study by thermochronological data to an average rate of ~2.6 °C/My below 500 °C. However, numerical simulations of the development of Fe–Mg profiles in Opx–Cpx pairs using this cooling rate grossly misfit the measured compositional profiles. Satisfactory simulation of the latter and low temperature thermochronological constraints requires a two-stage cooling model with a cooling rate of ~50–200 °C/ky from the peak metamorphic temperature of ~875 °C down to 450 °C, and then transitioning to very slow cooling with an average rate of ~2.6 °C/My. Similar rapid high temperature cooling rates (200–600 °C/ky) are also required to successfully model the compositional profiles in the Opx–Cpx pairs in the other samples of L5, L6 chondrites. For the H-chondrite samples, the low temperature cooling rates were determined earlier to be 10–20 °C/My by metallographic method. As in St. Séverin, these cooling rates grossly misfit the compositional profiles in the Opx–Cpx pairs. Modeling of these profiles requires very rapid cooling, ~200–400 °C/ky, from the peak temperatures (~810–830 °C), transitioning to the metallographic rates at ~450–500 °C. We interpret the rapid high temperature cooling rates to the exposure of the samples to surface or near surface conditions as a result of fragmentation of the parent body by asteroidal impacts. Using the thermochronological data, the timing of the presumed impact is constrained to be ~4555–4560 My before present for St. Séverin. We also deduced similar two stage cooling models in earlier studies of H-chondrites and mesosiderites that could be explained, using the available geochronological data, by impact induced fragmentation at around the same time. Diffusion kinetic analysis shows that if a lower petrological type got transformed by the thermal effect of shock impacts to reflect higher metamorphic temperature, as has been suggested as a possibility, then the peak temperatures would have had to be sustained for at least 10 ky and 80 ky, respectively, for transformation to the petrologic types 6 and 4. Finally, we present a model that reconciles textural data supporting an onion-shell parent body of H-chondrites with rapid cooling rate at high temperature caused by impact induced disturbance, and also discuss alternatives to the onion shell parent body model.

Keywords: Chondrites; Cooling rates; Impact; Parent body; Metamorphism

* Corresponding author.
E-mail address: ganguly@email.arizona.edu (J. Ganguly).

http://dx.doi.org/10.1016/j.gca.2016.07.030
0016-7037/

1. INTRODUCTION

Chondritic meteorites are generally accepted to be the most primitive and undifferentiated samples of the solar system. The known falls of these meteorites have been divided into three groups, viz. ordinary chondrites, carbonaceous chondrites and enstatite chondrites. The ordinary chondrites have been further subdivided into three chemical groups (H, L and LL) depending on their iron content. The samples in each chemical group are supposed to have been derived from the same parent body (asteroid) because of the similarity of their chemical properties (major element chemistry, oxygen isotope ratios) and oxidation state. Furthermore, samples within a specific chemical group are subdivided into different petrological types depending on the intensity of metamorphism, as reflected by their peak temperatures (T_{peak}) deduced from thermometric studies and textural maturity, with the intensity of metamorphism increasing in the order of the assigned numbers from 3 to 6.

It has been suggested, but also strongly debated, as reviewed by Ganguly et al. (2013), that the parent asteroid of the H-chondrites had an "onion-shell" structure in which each shell consisted of a specific petrologic type and was enclosed within a shell of lower petrologic type. This conclusion is based on cooling rates of samples of different petrologic types, as derived from thermochronological data (age vs. closure temperature relation, mostly below ~500 °C with sufficient spread of data) and their apparent compatibility with the calculated temperature–time (T–t) paths at different radial distances of an asteroid of 100 km radius, such as those calculated by Trieloff et al. (2003), Kleine et al. (2008) and Monnereau et al. (2013) (also see review in Ganguly et al., 2013). The parent asteroid was assumed to have been heated internally by the β-decay of ^{26}Al to ^{26}Mg and cooled by heat conduction (Trieloff et al., 2003; Kleine et al., 2008; Guignard and Toplis, 2015). Although an onion-shell parent body structure has been suggested only for H-chondrites, this should be a general feature of a parent body of approximately spherical shape if it was subjected to internal radiogenic heating with roughly uniform distribution of heat producing elements.

Ganguly et al. (2013) recently carried out a detailed thermometric and cooling rate studies of selected H chondrite samples on the basis of the compositions of coexisting ortho- and clino-pyroxenes (Opx and Cpx, respectively) in the metamorphic types 4–6 (H4: Forest Vale; H5: Allegan and Richardton; H6: Guarena and Kernouvé). They found the compositions of coexisting pyroxene pairs to be essentially homogeneous within the resolution of an electron microprobe (Cameca SX-100), and showed that preservation of these profiles requires orders of magnitude faster cooling rates (25–100 °C/ky) at high temperatures, commencing from the temperatures (750–850 °C) reflected by the pyroxene compositions, referred to henceforth as T_o, than those inferred from the thermochronological constraints at lower temperatures. Ganguly et al. (2013) thus developed a multistage cooling model that essentially reconciled all constraints on the cooling rates at both high and low temperatures, including the age vs. closure temperature (T_c) relations, as well as the metallographic cooling rates at intermediate temperatures (~550 °C), as determined by Krot et al. (2012). However, instead of using conventional T_c values that erroneously assume that a specific decay system has a fixed T_c, Ganguly et al. (2013) calculated the T_c values corresponding to the Pb–Pb ages of H chondrites (Göpel et al., 1994) by considering the effect of grain size, cooling rate and initial temperature at the onset of cooling, according to the extension of the classic work of Dodson (1973) by Ganguly and Tirone (1999).

To explain the very rapid cooling rate at high temperature, Ganguly et al. (2013) proposed that the parent body of H-chondrites had gone through a history of fragmentation when much of it was at or near peak temperatures as a result of radiogenic heating; the fragmentation process caused exposure of samples to surface or near surface conditions, and consequent rapid cooling. This was followed by reassembly of the fragmented material, thereby leading to slow cooling of the samples that were buried deeper under a blanket of asteroidal material. All fragmented material need not have been reassembled into a single secondary parent body, but some might have accreted to surface of other asteroidal body or gotten mixed with other asteroidal material to form new rubble pile type asteroids. The discovery of high grade materials (LL5 nd LL6) among the samples scooped from the surface of the asteroid Itokawa (Nakamura et al., 2011) lends credence to the model of Ganguly et al. (2013).

The primary purpose of this work is to extend the pyroxene cooling rate study of Ganguly et al. (2013) to L, LL and additional samples of H-chondrite samples and see if the results also reflect a history of fragmentation and reassembly, and if so to determine the timing of the possible fragmentation episode using available geochronological constraints. These results are then compared with those of Ganguly et al. (2013) for H-chondrite and two-stage cooling rates of mesosiderites (Ganguly et al., 1994) to develop a broader understanding of the impact and cooling histories of asteroidal parent bodies of meteorites, including the timing of the impacts. We also present constraints, on the basis of diffusion kinetic analysis, on the time period through which the peak temperatures of type 6 and 4 metamorphic types would have had to be sustained if some of these were produced by impact heating of the lower petrological types that equilibrated earlier at lower metamorphic temperatures, as suggested by Ciesla et al. (2013) from impact simulations. Finally, we present an integrated model that attempts to reconcile the evidence of metamorphism of the asteroidal parent body by internal radiogenic heating with the cooling rates deduced by Ganguly et al. (2013) and in this study.

2. COMPOSITIONAL PROFILES OF COEXISTING ORTHO- AND CLINO-PYROXENE PAIRS, THERMOMETRY AND COOLING RATES

2.1. Sample selection and thermometry

We acquired many samples of L and LL chondrites on loan from different sources, but most of them turned out to be too fine grained, presumably because of

shock-induced brecciation, to be suitable for the present study. The samples with relatively larger grain size that we selected are as follows: St. Séverin (LL6), ALH 85017 (L6), GRO 85204 (L6) and QUE 90202 (L5), QM USNM 15601 (H6), LAND USNM 6978-1 (H6) (ALH: Alan Hills; GRO: Grosvenor mountains; QUE: Queen Alexandra range; QM: Queen's Mercy; LD: Landreth Draw; USNM: United States National Museum). Of these, St. Séverin is of special interest since its cooling rate below ~500 °C has been constrained by geochronological methods (Min et al., 2013).

Recently van Niekerk et al. (2014) have reported results on the peak temperatures of several H6 and H5 chondrites that include six samples (four H6 and two H5) that were not part of the set of samples studied by Ganguly et al. (2013). The reported peak temperatures are comparable to those reported by the latter for H6 and H5 samples using the same thermometric calibration, and the coexisting clino- and ortho-pyroxene pairs, whose compositions were used to determine the peak temperatures, have been found to be homogeneous within the resolution of microprobe analysis. These results imply very rapid high temperature cooling rates, of the order of 10^2 °C/ky, similar to those deduced by Ganguly et al. (2013) for H5 and H6 samples. In this study, we also selected two more H chondrites, which were not included in the studies of either Ganguly et al. (2013) or van Niekerk et al. (2014), for detailed thermometric and cooling rate studies to see if they record any significantly different cooling history that may be compatible with their metamorphism and *in situ* cooling within an onion-shell parent body.

The paucity of clinopyroxene crystals in the chondrite samples made it very difficult to detect them under optical microscope. Thus, as in Ganguly et al. (2013), we detected coexisting pairs of Cpx and Opx grains by X-ray mapping in an electron microprobe (Cameca SX100). The selected pyroxene pairs were then analyzed by step scanning across the interfaces to determine the compositional profiles of the divalent cations. The conditions for the microprobe analyses are as follows: 20 kV accelerating voltage, 20 nA beam current with a focused beam of ~1 μm diameter, 20 s counts on the peak and 20 s on the background. Two examples of compositional profiles, along with the backscattered electron (BSE) images of coexisting pyroxene grains and traverse lines, are shown in Fig. 1. Special care was taken to ensure that a microprobe traverse line through an interface did not encounter any fracture or inclusion at or near the interface. For every sample, we measured almost as many profiles in Opx–Cpx pairs as there are in the thin section that had clean and fracture free linear segments of interfaces of sufficient lengths so that traverse lines could be drawn through those segments avoiding the potential problem arising from interference with the fractures and inclusions and diffusive exchange with the adjacent minerals. The traverse lines did not deviate by more than a few degrees from normalcy to the interface and we also ensured that these lines had least interference from fractures or inclusions within the interior of the crystals.

The peak metamorphic temperatures of the samples were determined according to two formulations: (a) the widely used two-pyroxene (2-Px) thermometric formulation of Anderson et al. (1993), which is based on extensive

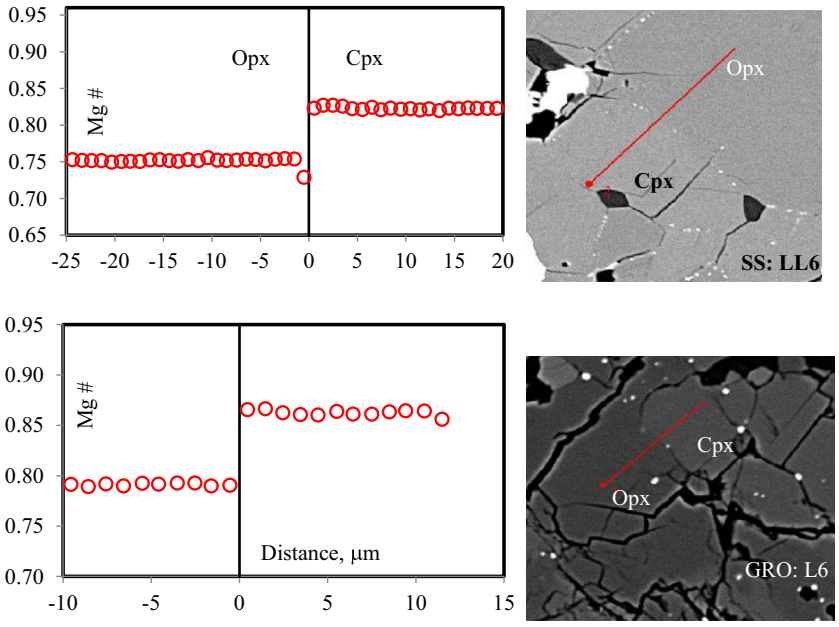

Fig. 1. Two representative profiles for Mg/(Mg + Fe) ratio (Mg#) in coexisting ortho- and clino-pyroxene (Opx–Cpx) pairs. The 2-Px pairs are in St. Séverin (SS: LL6) and Grossvenor Mountains (GRO: L6) meteorites. The backscattered electron images and traverse lines (red lines) corresponding to the profiles are shown on the right. The scale can be judged from the length of a profile on the left and that for a traverse on the BSE images (20 μm and 11.5 μm in the Cpx side of St. Séverin and GRO, respectively). (For visualization of colors, please see the web version of the article.)

experimental studies of Lindsley and co-workers (Lindsley, 1983 and references therein) on the compositional gap of Ca between Cpx and Opx in Ca–Fe–Mg–Mn system, and thermodynamic analysis of the data (b) Fe–Mg exchange thermometry between the two pyroxenes that was formulated by Ganguly et al. (2013) and is valid when $X(CaSiO_3)$ in Cpx $\geqslant 0.45$. For brevity, the formulation (a) will be referred to henceforth as 2-Px(Ca) and (b) as K_D(Fe–Mg). In our judgment, no other 2-Px(Ca) formulation matches the quality of the one used here because none is based on such an extensive body of experimental data that demonstrated attainment of equilibrium and rigorous thermodynamic analysis of the data.

We have also considered the thermometric formulations of Brey and Köhler (1990) which are based on experimental results at 10–60 kb in a four-phase lherzolite bulk composition. The temperatures obtained from K_D(Fe–Mg) and the formulation based on the transfer reaction En(Opx) = En (Opx) yield results in two test samples that differed by ~450 °C (633 vs. 1088 °C for St. Séverin; 635 vs. 1073 °C for Landreth Draw). Because of these discrepancies, we concluded that the formulations of Brey and Köhler (1990) based on the compositions of coexisting pyroxenes are not suitable at least for the thermometry of the meteorite samples that requires large extrapolation from the experimental pressure regime, especially since the correction factor for the pressure effect was not thermodynamically constrained. There might also have been other problems but a further discussion of the work of Brey and Köhler (1990) is beyond the scope of this study.

The thermometric results are summarized in Table 1 and illustrated in Fig. 2. For each sample, temperature was estimated for different Opx–Cpx pairs; for each pair, the average compositions of Cpx and Opx grains were estimated from spot analyses along line scans, such as illustrated in Fig. 1. For 2-Px(Ca) thermometer the computer program of Anderson et al. (1993) yields temperature estimates along with their respective 1σ errors. Thus, for the 2-Px(Ca) temperature we present (Table 1 and Fig. 2) the weighted mean temperature for each meteorite sample along with the standard deviation of the mean (we note, however, that there is very little difference between the weighted and unweighted means of 2-Px(Ca) temperatures). For the K_D(Fe–Mg) thermometric results, standard deviations of the means were estimated, using standard statistical method (e.g. Bevington and Robinson, 2003), by assuming that all temperature estimates in a given sample have the same standard deviation.

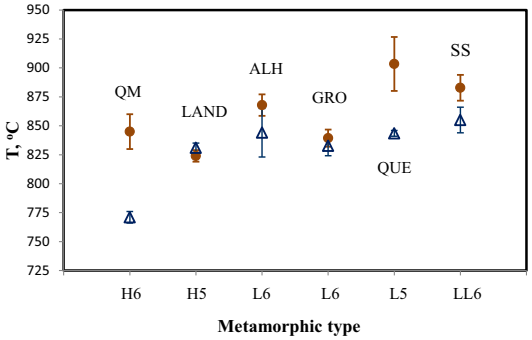

Fig. 2. Mean temperature vs. petrologic type of different H, L and LL chondrite samples according to 2-Px(Ca) (filled circles) and Fe–Mg exchange (open triangles) thermometers. The vertical error bars show the standard deviations of the means.

There is good agreement between the results from the two thermometric formulations, except for the samples QM (L6) and QUE (L5), but the temperature calculated from the 2-Px(Ca) thermometry (~825–900 °C) is higher than or almost the same as that from exchange thermometry (~770–855 °C), with an average discrepancy of 33 °C. Ganguly et al. (2013) did not find any significant difference between the peak temperatures experienced by H5 and H6 samples that they investigated. The same picture also emerges from the data illustrated in Fig. 2.

2.2. Determination of cooling rate: method and data

2.2.1. Outline of modeling protocol of compositional profiles in pyroxene diffusion couples

The high temperature cooling rates were calculated on the basis of the thermometric results and observed compositional profiles of the chosen meteorite samples. For the purpose of modeling the compositional profiles, we have taken the average of the results from the two thermometric formulations and treated those to be the temperatures that prevailed at the onset of cooling. These may or may not be the peak temperatures experienced by the sample, but if they were higher than those recorded by the mineral

Table 1
Summary of thermometric results and cooling rates for L-, LL-, and H-chondrites. Parenthetical numbers represent standard deviations of the estimated mean temperatures.

Meteorite	Type	T, °C (mean)		Average cooling rate	
		2-Px (Ca)	K_D (Fe–Mg)	High temp. (°C/ky)	Low temp.
St. Séverin	LL6	883 (9)	855 (11)	200[a]	2.6 °C/My (T_{tr} ~ 450 °C)
ALH 76001	L6	868 (9)	844 (21)	200	
GRO 90202	L6	839 (9)	833 (8)	200	
QUE 90202	L5	903 (23)	843 (2)	600	
QM	H6	845 (15)	771 (5)	200	10 °C/My (T_{tr} ~ 450–500 °C)
LD	H5	824 (5)	831 (4)	400	20 °C/My (T_{tr} ~ 450–500 °C)

ALH: Allan Hills; GRO: Grosvenor Mountains; QUE: Queen Alexandra Range; QM: Queen's Mercy; LD: Landreth Draw. T_{tr}: transition temperature.

[a] A factor of ten reduction is possible considering the full range of diffusion data for clinopyroxene.

compositions, then the samples must have been held long enough at the lower temperatures to achieve compositional homogeneity, as observed, and cooled subsequently. Resetting of core composition of minerals during cooling leads to conspicuous zoning from the core to the rim (the compositional difference between core and rim is what drives resetting of core composition), as demonstrated below, and in other studies, as for example Ganguly et al. (2013, Fig. 6). Thus, since the compositional profiles have been found to be almost uniform within the resolution of microprobe spot analysis, we assume that the coexisting pyroxenes were completely homogenized at the onset of cooling from the temperatures recorded by their compositions.

The diffusive exchange of Mg and Fe between coexisting Opx and Cpx has been treated in terms of a binary interdiffusion process. The solubility of Ca in Opx is so low (Ca < 1.7% of the divalent cations) that the effect of Ca on the diffusion of Mg and Fe could be neglected. As noted by Ganguly et al. (2013), equilibrium Fe–Mg fractionation between the two pyroxenes during cooling would have caused their Mg/(Mg + Fe) ratio or Mg# at the interface to recede from one another, and consequently the resulting zoning profiles near the interface would have been damped in microprobe spot analyses due to spatial averaging or convolution effects, which depend on the size of the excitation volume within a sample around the center of the electron beam. The method for correcting for the convolution effect was developed by Ganguly et al. (1988) and has been incorporated into the numerical code developed by Ganguly et al. (2013), which is also used in this study for modeling the evolution of compositional profile for prescribed cooling rate and T_o. As shown by Ganguly et al. (2013) as well as in the simulations carried out in this study, convolution correction does not significantly diminish the difference between profiles that resulted from different cooling rates; for example, profiles developed by cooling at 25 °C/ky is clearly distinguishable from that at 100 °C/ky after convolution correction (Ganguly et al., 2013: Fig. 5). Also convolution of completely homogeneous profiles in two sides of an interface is typically restricted to ~1 μm from the interface at the analytical conditions used in this study, and leads to a decrease in the difference between its true concentrations in the two sides within this domain (Ganguly et al., 1988: Fig. 4). The details for the two-phase binary diffusion modeling protocol and mathematical framework have been given in the study of Ganguly et al. (2013). Thus, only a brief and non-mathematical description of the procedure is given below.

Assuming homogeneous initial compositions of both Opx and Cpx, the evolution of compositional profiles in a coexisting pair was simulated by solving 1-D diffusion equation for a binary system in Cartesian coordinates. Since diffusion was limited to within a few microns from the interface, and the traverse lines for microprobe analyses were always much further away from any other grain boundary, 1-D simulation is appropriate. The compositions of the two minerals at the interface were assumed to satisfy the distribution coefficient of Fe and Mg (K_D(Fe–Mg)) as a function of temperature. An additional boundary condition is imposed by assuming that there is no interface leaking so that the flux of a component out of one mineral equals that into the other mineral in a two-pyroxene couple. Since there is no analytical solution to the diffusion problem that we would be dealing with, a finite difference scheme following the widely used Crank-Nicolson implicit method (Crank, 1975), which is unconditionally stable, was used to solve the diffusion equation. The quenched compositional profiles calculated for a prescribed cooling (T–t) path were then corrected for spatial averaging effect and compared with the measured profiles. The process was repeated until a satisfactory match was found between the two sets of profiles.

2.2.2. Sources of diffusion data

The different sets of diffusion data used in the modeling of concentration profiles in this study are illustrated in Fig. 3. The primary source of diffusion data are, however, the same as in Ganguly et al. (2013), namely Zhang et al. (2010) for Cpx and Ganguly and Tazzoli (1994) for Opx, but with some modifications, as discussed below. The former data set is for diffusion of Mg instead of the interdiffusion of Fe and Mg. On the basis of the difference between the available diffusion coefficients (D) of Fe and Mg in other minerals, Ganguly et al. (2013) argued that use of D(Mg) for D(Fe–Mg) in Cpx is unlikely to make significant difference in the calculation of cooling rates. Also, as in their study, we have used D(Mg) data parallel to the b-axial direction (D(Mg)//b), which, according to Zhang et al. (2010), is the slowest diffusion direction (among those defined by the crystallographic axes) in Cpx. According to these data, there is very little difference for diffusion parallel to a and b axial directions, but D(//c) is ~5 times greater than D(//b) at 800 °C, with the difference increasing with decreasing temperature (Fig. 3). The D(Fe–Mg) in Opx given by Ganguly and Tazzoli (1994) is derived from the

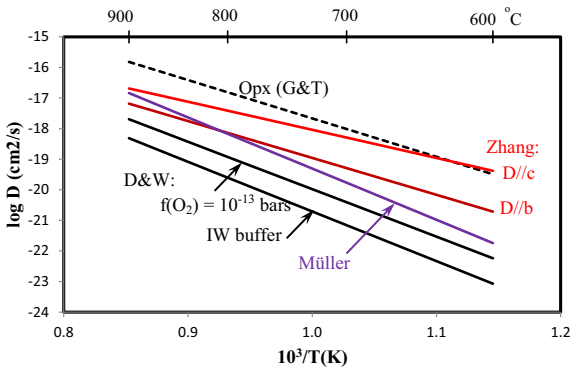

Fig. 3. Summary of diffusion used in modeling Mg# profiles in Opx–Cpx pairs. All solid lines represent diffusion data for clinopyroxne (Cpx) whereas the dashed line represents the D(Fe–Mg) data of Ganguly and Tazzoli (1994) in orthopyroxene, averaged for diffusion parallel to c and b axial directions. The explanation for Cpx diffusion data is as follows; solid red: D(Mg)// c and D(Mg)//b (upper and lower lines, respectively) of Zhang et al. (2010); violet: D(Fe–Mg)//c of Müller et al. (2013); black: D((Fe, Mn)–Mg) of Dimanov and Wiedenbeck (2006) at $f(O_2) = 10^{-13}$ bars (upper line) and corrected for $f(O_2)$ variation with T along IW buffer (lower line). (For visualization of colors, please see the web version of the article.)

data for Fe–Mg order–disorder kinetics between the M2 and M1 crystallographic sites and, as discussed by them, represent the average of inter-diffusion parallel to the *c* and *b* crystallographic axes. We found that the model fits to the concentration profiles in this study for one sample, St. Severin, improved if D(Fe–Mg) of Opx given by Ganguly and Tazzoli (1994) is reduced by a factor of 5; thus, this adjustment, which is within the uncertainty of the data, was used for all simulations presented in this study. However, for other samples, there is practically no difference between cooling rates retrieved from using the modified and original diffusion data for Opx. The use of the above set of diffusion data should yield roughly a lower bound for the cooling rate required to produce an observed set of Fe–Mg profiles in a Opx–Cpx pair if the choice of diffusion data is restricted to Zhang et al. (2010) for Cpx and Ganguly and Tazzoli (1994) for Opx.

Dimanov and Wiedenbeck (2006) determined quasi-binary (Fe,Mn)–Mg inter-diffusion data in natural Cpx as a function of temperature and $f(O_2)$ at 1 bar, and presented an Arrhenian relation at fixed $f(O_2)$ of 10^{-13} bars (Fig. 3). However, variation of $f(O_2)$ in nature is usually buffered by mineral assemblages that roughly follows the $f(O_2)$–T relation of a solid oxygen fugacity buffer like that of iron-wüstite (IW). Thus, and also since $f(O_2)$ of chondritic meteorites is no higher than the latter, we have adjusted the diffusion data of Dimanov and Wiedenbeck (2006) for variation of $f(O_2)$ along the IW buffer with changing temperature according to the method presented in Posner et al. (2016) and $\log f(O_2)$ vs. T relation for the buffer from O'Neill (1988). The derived $\log D$ vs. $1/T$ relation, which is illustrated in Fig. 3, has the following Arrhenius parameters: $D_o = 3.39(10^{-9})$ cm^2/s and Q (activation energy) = 311 kJ/mol.

Recently Müller et al. (2013) determined D(Fe–Mg) in Cpx for diffusion parallel to the *c*-axial direction, which is intermediate between those of Zhang et al. (2010) and Dimanov and Wiedenbeck (2006) parallel to *c*-axis (Fig. 3). However, in contrast to the latter study, Müller et al. (2013) did not find any dependence of D on $f(O_2)$. They explained this on the basis of the fact that the Cpx crystals used in their diffusion studies are relatively Al rich (Al(VI) = 0.05) compared to those used by Dimanov and Wiedenbeck (2006) (Al(VI) = 0.00). This presumably led to a nearly constant concentration of octahedral point defects in their Cpx crystals, irrespective of the variation of $f(O_2)$; in other words, the extrinsic point defects created by Al substitution in the octahedral site swamped the variation of point defect concentration resulting from change of $f(O_2)$.

We have considered the effect of variation of the diffusion data for clinopyroxene on the results of cooling rate retrieved from modeling Opx–Cpx Mg# profiles. This is discussed in the Section 2.3.4.

2.3. Results

The results for the modeling of measured compositional profiles of Mg in the Opx–Cpx pairs in different L, LL and H chondrite samples, along with the available constraints on cooling rates of some of the samples (St. Séverin: LL6 and H chondrites) from thermochronological and metallographic studies, are discussed below. For each sample, we have simulated the profile(s) that showed the least scatter of microprobe data along the chosen traverse across an interface. However, with regard to the development of zoning near the interface, the measured profiles in a given sample are very similar.

2.3.1. St. Séverin (LL6)

Min et al. (2013) constrained the single grain (U–Th)/He ages from a number of merrillite and chlorapatite grains separated from St. Séverin (SS). They combined those data with the Pb/Pb phosphate age (Bouvier et al., 2007), whole rock (WR) $^{40}Ar/^{39}Ar$ ages (Hohenberg et al., 1981, with revision as discussed by Min et al., 2013) and WR (U–Th)/He ages (Wasson and Wang, 1991), along with the commonly accepted values for the closure temperatures (T_c) for each decay system, to construct a temperature–time (T–t) path for cooling of St. Séverin below 500 °C. The age vs. T_c data for the different decay systems, which are illustrated in Fig. 4 by filled symbols, indicate nonlinear cooling below ~500 °C, with an average rate of ~2.6 °C/My, as estimated by Min et al. (2013).

We have fitted the T_c vs. age data by a nonlinear cooling function, $1/T = 1/T_o + \eta t$, where T_o is the temperature (K) at the onset of cooling and η is a constant with dimension of $K^{-1}\ t^{-1}$. This cooling model has been used earlier by other workers (e.g. Dodson, 1973; Ganguly, 1982; Ganguly et al., 2013), and was called an "asymptotic model" by Ganguly (1982). The fitted relation, which is illustrated in Fig. 3 by a solid red line and corresponds to $\eta = 6(10^{-6})$/K-My,

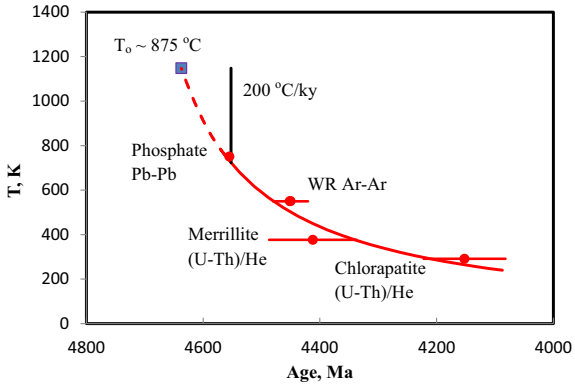

Fig. 4. Thermochronological data (T_c vs. age: filled red circles) for St. Séverin as summarized by Min et al. (2013). The original sources of the data and uncertainty of the ages (in My) are as follows: phosphate (Bouvier et al., 2007; ±0.1); Ar–Ar (Hohenberg et al., 1981, ±30); merrillite (Min et al., 2013; 75); chalcopyrite (Min et al., 2013; 70). The data have been fitted by an asymptotic cooling model (solid red line), $1/T(K) = 1/T_o(K) + \eta t$, with $\eta = 6$ (10^{-6})/K-My, and extrapolated to the peak temperature, 875 °C, as estimated in this study (Table 1). The nearly vertical line (black) shows the high temperature segment of the two-stage cooling model needed for the successful simulation of the compositional profiles in Opx–Cpx pairs, preserving the geochronological constraints. (For visualization of colors, please see the web version of the article.)

has been extrapolated (dashed line) to 875 °C that represents the average of 2-Px(Ca) and K_D(Fe–Mg) thermometric results for St. Séverin (Table 1). We note, however, that the extrapolated T–t path yields an age of 4637 Ma, which is older than the age of the solar system by ~70 Ma. This problem, in itself, is suggestive that the T–t path constrained by the thermochronological data below ~500 °C cannot be extrapolated to the peak temperature.

We simulated the evolution of Mg-profiles of Opx–Cpx pairs in St. Séverin as a function of time, assuming continuous cooling from 875 °C according to the above asymptotic model. The simulated quenched profiles are compared with the measured data in Fig. 5. It is obvious that there is a gross mismatch between the simulated and measured profiles, irrespective of the choice of D(Mg) data for Cpx, that leads us to conclude that the pyroxene profiles could not have developed by cooling along a T–t path obtained from extrapolation of that constrained by the geochronological data below ~500 °C.

To obtain a satisfactory match, as judged by visual inspection, between simulation and observation, we adopted a two-stage cooling model in which the sample is assumed to have-cooled rapidly from the peak temperature (875 °C) down to a transition temperature, T(tr), below which the cooling followed the asymptotic T–t path that is constrained by the geochronological data (Fig. 4). The results are illustrated in Fig. 6. In each case (also Figs. 7 and 8) the black dashed lines represent the calculated Mg-profile and the solid red lines represent the convolution of the calculated profile due to the spatial averaging effect in microprobe spot analyses at the imposed analytical conditions. The convolved profiles are the ones that should be compared with the microprobe data.

The most successful simulation of the Mg# vs. distance data shown in Fig. 5 is illustrated in Fig. 6a) for which we used a constant cooling rate (CR) of 200 °C/ky above 450 °C and a nonlinear T–t path at lower temperature that fits the geochronological constraints (Fig. 4). The cooling rate at any temperature below 450 °C is given by ηT^2 with T in Kelvin and $\eta = 6(10^{-6})$/K-My; thus, at 400 °C, CR = 2.7 °C/My that is essentially the same as the average cooling rate (2.6 °C/My) determined by Min et al. (2013). There is a slight misfit between the simulated and measured concentration profiles on the Opx side of the interface (ΔMg# = 0.013), but we could not obtain a better match between the two profiles by varying diffusion parameters and initial temperatures within their permissible limits,

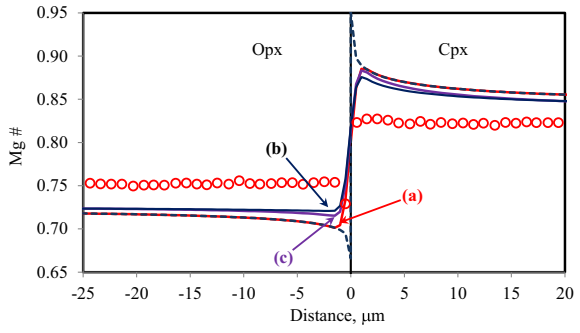

Fig. 5. Comparison of the measured Mg# data vs. distance (open circles) in Opx–Cpx pair in St. Séverin (LL6) with those developed as quenched profiles in numerical simulations using an asymptotic cooling model, $1/T = 1/T_o + \eta t$, with $\eta = 6(10^{-6})$/K-My, which is derived from the low-temperature (<500 °C) thermochronological data (Fig. 3). In all simulations, D(Fe–Mg) for Opx is from Ganguly and Tazzoli (1994), reduced by a factor of 5, whereas three sets of diffusion data have been used for Cpx (as discussed in the text). Dashed line: simulated profile using D(Mg)//b of Cpx from Zhang et al. (2010), whereas the solid red line (a) is the calculated convolution of the simulated profile due to the spatial averaging effect in microprobe spot analyses. The two other solid lines are also convolved quenched profiles corresponding to different diffusion data for Cpx: (b) D(Fe–Mg)//c by Müller et al. (2013) and (c) D(Mg)//b from Zhang et al. (2010), reduced by a factor of 4. (For visualization of colors, please see the web version of the article.)

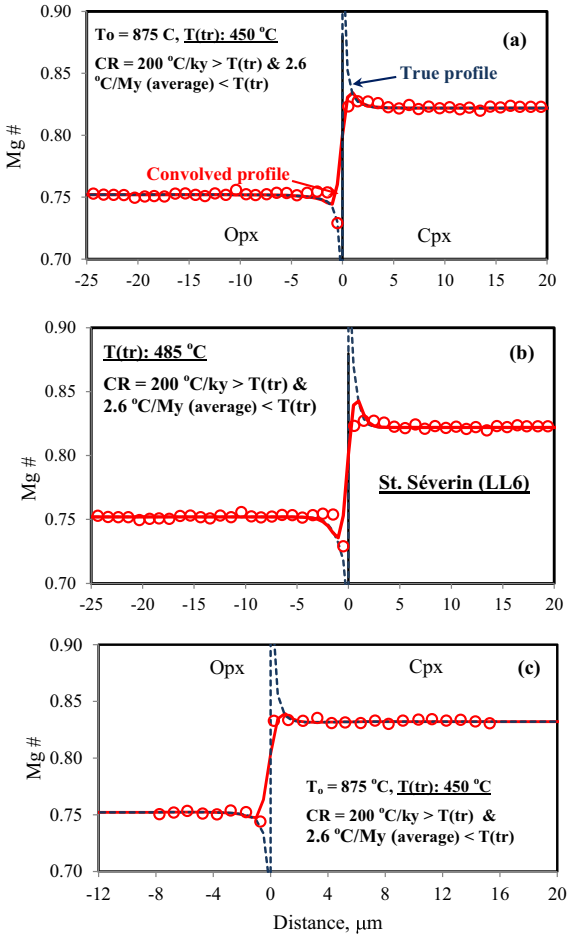

Fig. 6. Numerical simulation of the development of compositional profiles in Opx–Cpx pairs in two Opx–Cpx pairs in St. Séverin (LL6) by two stage cooling process with two different transition temperatures: 450 °C for (a) and (c) and 485 °C for (b); the second stage cooling follows the thermochronologically constrained non-linear T–t path illustrated in Fig. 4. Dashed line: simulation (final true profile), solid line: calculated convolution of the simulated profile accounting for the spatial averaging effect in microprobe analyses. A range of simulations have been carried out to find the best match to the Mg# vs. distance data (open circles) for each sample. The measured profiles in (a) and (b) are the same; the traverse line is shown in the BSE image in Fig. 1 (SS: LL6).

and T(tr) (see further discussion in section in Section 2.3.4). We could not obtain an equally satisfactory match between the simulated and measured profiles, with the former corrected for convolution effect, by setting the transition temperature (T(tr)) much higher. A simulation with T(tr) = 485 °C, keeping the T–t relation at higher and lower temperature the same as above, is shown in Fig. 6(b). The quality of fit to the measured Mg-profile did not change by varying the high temperature cooling rate between 200 °C/ky and 800 °C/ky (there is no flexibility for the low temperature T–t path because of the geochronological constraints). Fig. 6(c) shows another successful simulation of Mg profile in a different Opx–Cpx pair in St. Séverin using the same two-stage cooling model used in the simulation illustrated in Fig. 6(a).

2.3.2. L6 and L5 chondrites

Selected successful simulations of the measured Mg-profiles in Opx–Cpx pairs in three L6 and L5 chondrites, GRO (L6), ALH (L6), QUE (L5), are illustrated in Fig. 7 (the abbreviations of all meteorite names are given in Section 2.1 and Table 1). There are good matches between the measured and the simulated convolved profiles for the following cooling rates: 200 °C/ky for GRO and ALH and 600 °C/ky for QUE. These simulations do not imply that the samples cooled at constant rates all through. As in the case of St. Séverin, the cooling rates could have changed at some low temperatures. If they did, then the transition temperature would depend on the rate of cooling in the lower temperature regime. For example, if the low temperature cooling rate was 2.6 °C/My, similar to the average low temperature cooling rate of St. Séverin, then the successful simulations of the Mg profiles in the Opx–Cpx pairs in this group of L5 and L6 samples require the above high temperature cooling rates to continue down to ~450 °C, just as in the case of St. Séverin.

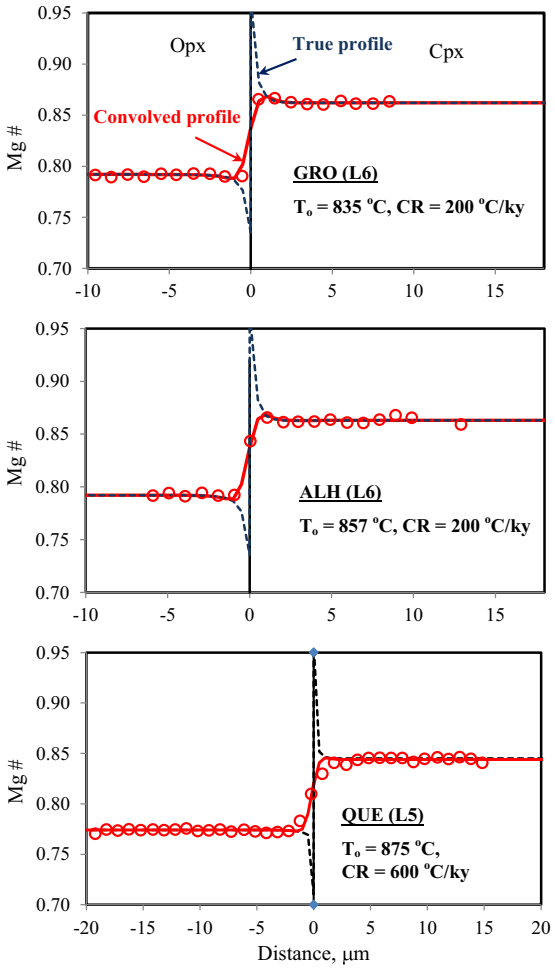

Fig. 7. Successful simulations of compositional profiles (Mg#) in L6 and L5 chondrites with T_o (constrained by thermometry) and cooling rates indicated in the panels. For a change of cooling rate at low temperature to 2.6 °C/My, as in St. Séverin (LL6, Fig. 6), the high temperature cooling rates of the samples would have to continue down to 450 °C. Solid and dashed lines: See Fig. 6 for explanation.

2.3.3. H chondrites

Using metallographic method (central Ni composition of taenite grains following Wood, 1967), Scott et al. (2014) determined the cooling rates of the H chondrite samples, QM (H6) and LD (H5) to be 20 °C/My and 10 °C/My, respectively. The metallographic cooling rates are, however, applicable to temperatures around 550 °C. Use of the above cooling rates to model the Mg profiles of Opx–Cpx pairs in the H chondrite samples, commencing at temperatures recorded by the pyroxene compositions (QM: ~810 °C;

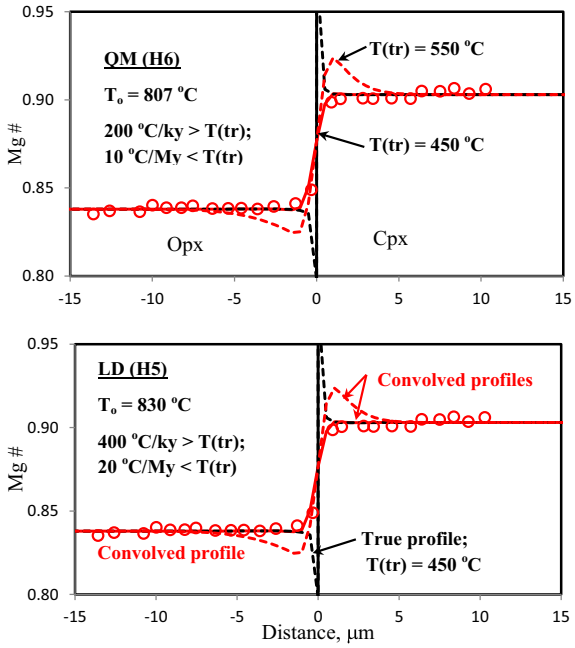

Fig. 8. Numerical simulations of compositional profiles (Mg#) in H6 and H5 chondrites with two-stage cooling models. Convolved profiles with transition temperature of 450 °C and 550 °C are indicated by solid and dashed red lines, respectively. The low temperature cooling rates are constrained by metallographic data. (For visualization of colors, please see the web version of the article.)

LD: ~830 °C) lead to quenched Mg profiles that grossly misfit the measured ones. Accepting the metallographic cooling rates, successful simulations of the measured Mg profiles of Opx–Cpx pairs require at least a two-stage cooling model, with ~200 °C/ky for QM and ~400 °C/ky for LD at high temperature and transitioning to the respective metallographic cooling rates at ~450 °C. The successful simulations of the Mg profiles in two Opx–Cpx pairs in QM and LD, using the two-stage cooling models, are illustrated in Fig. 8. Also shown are profiles with a transition temperature (T(tr)) of 550 °C that fail to match the compositional profiles; variation of high temperature cooling rate does not improve the match with the observed profiles. To obtain satisfactory match between the simulated and measured profiles with a T(tr) ~ 550 °C, the metallographic cooling rates need to be revised upward by an order of magnitude. However, an equally good match between the simulated and measured profiles as those illustrated in Fig. 8 with T(tr) of 450 °C could be obtained with a T(tr) of 500 °C if the D(Cpx)//b is reduced by a factor of 4. As discussed below, this adjustment of D(Cpx)//b is within the uncertainty of the experimental data.

The two stage cooling model developed above to reconcile the metallographic cooling rate at low temperature with the orders of magnitude faster cooling rates at high temperature (constrained by the nearly homogeneous compositions of Opx–Cpx pairs) is qualitatively similar to that deduced by Ganguly et al. (2013) for Guarena, which is a H6 chondrite. However, in the latter study, the T(tr) between the rapid high temperature cooling rate and the much slower metallographic rate at lower temperature was found to be ~650 °C. The substantial difference between the T(tr) values of Guarena and the H chondrites studied in this work prompted us to re-examine the simulations in Ganguly et al. (2013). It was found that in the simulation illustrated in their Fig. 8, the low temperature metallographic cooling rate was mistakenly entered as 15 °C/ky instead of 15 °C/My. Correcting for this error, we find that the T(tr) for Guarena is ~500–550 °C, given the uncertainty of the diffusion data, as discussed above (factor of 4–5), and allowing for variation of metallographic cooling rate between 15 and 30 °C/My (lowering the rate of second stage cooling pushes T(tr) downwards to avoid resetting of the concentration profiles; the effect of longer time, which favors resetting, is compensated by slower diffusion kinetics at lower temperature). Thus, the transition temperatures to the slow metallographic cooling rates of all H5 and H6 samples that we have studied so far fall in the range of ~500–550 °C.

In contrast to the rapid high temperature cooling rates deduced in this study and Ganguly et al. (2013) for H6 samples (of the order of 10^2 °C/ky), the cooling rate in an onion-shell model at ~40 km radial distance, which is considered to be the appropriate location of H6 chondrites in a spherical parent body of 100 km radius and heated internally by ^{26}Al decay, is 10–20 °C/My in the temperature range of 800–500 °C (Kleine et al., 2008).

2.3.4. Effect of change of diffusion data and initial conditions on cooling rate calculations

The Fe–Mg diffusion data for Cpx illustrated in Fig. 3 show large variations, which are due to differences in point defect concentrations, as discussed by Müller et al. (2013), and also experimental problems including the measurement of the diffusion profiles. We are, however, not in a position at this stage to analyze the experimental problems associated with the individual studies. At any rate, we consider here the effect of different sets of diffusion data on the values of retrieved cooling rates.

First, we note that D(Fe–Mg) of Cpx parallel to the c-axial direction determined by Müller et al. (2013) is much slower than D(Mg) determined by Zhang et al. (2010) (Fig. 3). It is, however, quite close to D(Mg)//b determined by the latter that we used to model the Opx–Cpx Mg# profiles (Figs. 6–8). The reason for this discrepancy remains unclear. However, because of this discrepancy between two data sets for diffusion data parallel to the c-axis, we considered the possibility that D(Mg)//b in Cpx could be smaller than that given by Zhang et al. (2010), and tested the effect of lowering the diffusion coefficient by a factor of four on the simulation of a Mg-profile of a Opx–Cpx pair in St. Séverin and H chondrites. The reduced D(Mg)//b is a reasonable lower limit of the data by Zhang et al. (2010), considering the errors of the Arrhenius parameters of their data. We modeled the Mg# profiles in St. Severin illustrated in Fig. 6(c) with the adjusted diffusion data for Cpx and found that good match between the simulated and observed profiles could be obtained, by using high-T cooling rate of 50–200 °C/ky, followed by a second stage slow non-linear cooling (average 2.6 °C/My) below 450 °C; the quality of simulation is about the same as illustrated in Fig. 6(c) except that the there is a slightly greater mismatch between the first point from the interface in the Opx side and the simulated Mg# (ΔMg# = 0.015). The use of the diffusion data of Mueller et al. (2014) yields almost exactly the same simulated profiles for the same cooling rates as with the D(Mg)//b data of Zhang et al. (2010), reduced by a factor of 4.

We have tested the effects of reduction of the data of Zhang et al. for D(Mg)//b by a factor of 4 and of D(Fe–Mg) for Opx of Ganguly and Tazzoli (1994) by a factor of 5 for the simulations in Ganguly et al. (2013). To recapitulate, it has been found in this study that the downward adjustment for the Opx diffusion data improves the match for the profiles in St. Séverin (Fig. 6), but other profiles that are essentially flat are insensitive to this change. The Mg# profiles in Opx–Cpx pairs in the samples studied by Ganguly et al. (2013) have been found to be insensitive to the adjustment of the diffusion data for Opx, but the downward adjustment for the Cpx data leads to a lowering of cooling rate by a factor of around five from that determined by Ganguly et al. (2013). This change does not, however, affect any of the conclusions of Ganguly et al. (2013) since the cooling rates still remain a few orders of magnitude larger than the available cooling rate data at low temperature cooling. For the Opx-spinel pairs in Ganguly et al. (2013), the retrieved cooling rates are reduced by a factor of five, i.e. to 10 °C/ky from 50 °C/ky, if we use the adjusted diffu-

sion data for Opx. Interestingly, the reduced cooling rate is the same as that determined by Krot et al. (2012) from metallographic data.

We have also used the D(Fe–Mg) data of Dimanov and Wiedenbeck (2006), adjusted for f(O_2) variation along IW buffer (Fig. 3) to model the Opx–Cpx Mg# profile of St. Séverin illustrated in Fig. 6(c). We tried many combinations of high-T cooling rates and T(tr), but could find a good match, very similar to that shown in Fig. 6(c), to the Mg# profiles of the pyroxenes only after reducing the D(Fe–Mg) of Opx by a factor of 300 and using a high-T cooling rate of 20 °C/ky along with a T(tr) of 580 °C. The T–t path below the T(tr) is the same as that constrained by the thermochronological data and used in all simulations of the Opx–Cpx Mg# profiles of St. Severin.

We have also tested the effect of variation of initial temperatures (T_o) on the values of retrieved cooling rates. It should be obvious that increasing T_o would necessitate faster cooling rates to produce the same or very similar profiles, since the diffusion coefficients become larger, and would thus strengthen our model of parent body history based on rapid high-T cooling rates that we have calculated. Thus, we focus only on testing the effect of lowering T_o within permissible limits of the thermometric results. For this exercise, we selected two samples, St. Séverin and Queen's Mercy. From the thermometric results summarized in Table 1 and illustrated in Fig. 2, the initial temperatures of these samples could be lowered by no more than 25 °C and 37 °C, respectively, from the temperatures used in the simulations in Figs. 6 and 8(a). These limiting values correspond to the temperatures calculated from the K_D(Fe–Mg) thermometry. The adjusted temperatures represent, respectively, 43 °C and 75 °C lowering of the temperatures obtained from the 2-Px(Ca) thermometric formulation (Lindsley, 1983; Anderson et al., 1993) that were very carefully calibrated, as discussed above, and also has been tested extensively in studies of terrestrial samples from both metamorphic and igneous rocks. Thus, we do not feel that any further lowering of the initial temperatures of the sample is justified. The simulations of the selected profiles using the new initial temperatures yield essentially the same cooling rate as before. In summary, the variation of diffusion parameters and initial temperatures within permissible limits do not change the overall scenario of very rapid cooling (of the order of 10–10^2 °C/ky) at high temperature.

3. DISCUSSION

From the results presented above, it should be obvious that after allowing for the uncertainties in the diffusion parameters and initial temperatures, modeling of the pyroxene compositional profiles of all H, L and LL chondrite samples studied so far yield high-T cooling rates of the order of 10–10^2 °C/ky. Göpel et al. (1994) drew attention to the petrographic features of H chondrites, namely small grain size of ferromagnesian silicates, preservation of clinobronzite and striated pyroxene, and survival of polycrystalline taenite in H chondrites that, as emphasized by them, "require a very short time (days or weeks) above 1100 K and fast cooling" (1100 K is close to the peak temperatures of the samples studied in this work). Use of low-T cooling rate constrained independently by metallographic methods and/or thermochronological data to model Mg# profiles in Opx–Cpx pairs grossly misfit the measured profiles (Fig. 4; Ganguly et al., 2013: Fig. 5). Thus, at least for the samples that show slow low-T cooling of the order of several to few tens of degrees per My, a two or multi-stage cooling model is required to fit all constraints on the T–t paths.

We discuss below additional implications of the cooling rate studies, temporal constraint on the feasibility of shock resetting of metamorphic grades, and finally present a synthesis of cooling rate and textural data of H chondrite to develop a model for metamorphism and shock history.

3.1. Comparison of the cooling histories of chondrite groups and mesosiderites and implications

The rapid high temperature cooling rates (of the order of 200–600 °C/ky) of the L, LL and H chondrites that we have determined in this study are comparable to the cooling rates deduced by Ganguly et al. (2013) for H chondrites. In an earlier study on mesosiderites, Ganguly et al. (1994) found that the Fe–Mg profiles in Opx–Opx diffusion couples, which formed in some samples as a consequence of overgrowth of Opx on earlier formed crystals, imply very rapid cooling rate, ~1–10 °C/ky, from the peak temperature of 1120–1150 °C. These cooling rates are in sharp contrast to the much slower low temperature cooling rates (fraction of a degree to the order of 10^2 °C/My, depending on the temperature) deduced from Ar–Ar ages and corresponding closure temperature, T_c (Bogard et al., 1990), metallographic data (Powell, 1969, as modified by Ganguly et al., 1994) and the quenched Fe–Mg ordering states of orthopyroxenes (Ganguly et al., 1994). Ganguly et al. (1994), thus, proposed a two-stage cooling model for the mesosiderites with a transition temperature between 500 °C and 800 °C.

Geochronological data provide constraints for the timing of transitions from rapid high temperature cooling to orders of magnitude slower cooling rate at lower temperatures for the three groups of meteorites, H and LL chondrites and mesosiderites. The T vs. age data for St. Séverin (LL6) illustrated in Fig. 4 and those for H chondrite (Ganguly et al., 2013, Fig. 11) show that the transition had taken place ~4555 and 4560 My before present, respectively. The timing for the T(tr) in the cooling path of the mesosiderites may be constrained from the Sm–Nd mineral ages (4470 ± 20 Ma), as determined by Prinzhofer et al. (1992) and interpreted by them to have been reset by 90 Ma. Sano et al. (2011) showed that this resetting is compatible with that expected from the cooling model of mesosiderite developed by Ganguly et al. (1994), with all resetting taking place in the lower temperature slow-cooling limb commencing at ~770 °C, since the time spent by the rock between the T_{peak} and T(tr) is too small to cause any significant resetting. Thus, the timing of the T(tr) for the mesosiderites becomes 4560 (±20) Ma, which is similar to that deduced for the H and LL chondrites.

The rapid high temperature cooling of the H4-6 (Ganguly et al., 2013; this study), L5 and LL6 samples (this

study), as well as mesosiderites (Ganguly et al., 1994), imply exposure of the samples to surface or near surface conditions. This might have been caused from impact induced fragmentation of the parent asteroid (Ganguly et al., 2013) or flow of material from the interior following one or more impacts (Ciesla et al., 2013). The timing of the impacts must have been only slightly before the T(tr) of the two-/multi-stage cooling models discussed above since very little time would have been spent between T_o and T (tr) because of the very rapid cooling rate within this temperature interval. Thus, we conclude that the impacts of the asteroidal parent bodies of chondrites (LL, L and H) and mesosiderites had taken place between ~4.55 and 4.58 Ga. Although we have not carried out an exhaustive study of the cooling history of meteorites, we note that numerical simulations of asteroidal impacts by Davison et al. (2013) suggest that collision rates among asteroids were highest during the first 100 Myr of solar system with a peak activity in the first 5–20 Myr. Our results for the timing of the suggested impact induced disturbance of chondrite (H, L and LL) and mesosiderite parent bodies fall within the period of peak impact activity suggested by Davison et al. (2013).

3.2. Transformation to higher temperature petrologic type by shock effects: constraints on the time scale of peak thermal condition

Ciesla et al. (2013) presented simulations of thermal profiles as a function of radial distance of an asteroid of 100 km radius that formed 2.2 My after CAI formation and was heated internally by the decay of ^{26}Al to ^{26}Mg, and superposed on these the thermal effects of shock by an impactor 10 My after the formation of the asteroid when the temperature was past the peak condition but still high (~1200–800 K) at 80–95 km from the center. The impactor was chosen to be 10 km in diameter colliding with the target at 4 km/s speed. Ciesla et al. (2013) suggested the possibility that such impact process could have led to the transformation of rocks in the target to higher petrologic types as a direct result of impact heating and/or burial of pristine crustal rock under hot rocks exhumed from depths. However, the transformation of petrologic type depends not only on temperature, but also on the residence time of a rock at the perturbed temperature. This point was recognized but not addressed by the Ciesla et al. (2013). We provide below quantitative constraints on the time scale for transformation of petrologic type through diffusion kinetic modeling.

We assume that the thermal effect of an impact instantly resets the surface concentrations of Opx–Cpx pairs, satisfying the distribution coefficient K_D(Fe–Mg) at the impact induced temperature. Cpx grains are rare, and are typically embedded in a matrix in which Opx is a major component; also all Opx grains in a sample have been found to have essentially the same composition. Thus, we assume that Opx grains surrounding a Cpx grain had served as a homogeneous infinite reservoir because of relatively rapid grain boundary diffusion, as demonstrated experimentally by Liermann and Ganguly (2001). In this case, we can calculate the minimum time (t) needed to equilibrate the interior of a Cpx grain by assuming a spherical geometry, for which $t \sim 0.4(r^2/D)$, where r is the grain radius (Crank, 1975, Fig. 6.1).

We have not determined the orientations of the traverse lines for profile measurements. However, even if the orientations were known, we do not have adequate diffusion data to determine the diffusion coefficients parallel to the three principal axes of diffusion (only the b direction in Cpx constitutes such an axis) that are needed to calculate diffusion coefficient parallel to an arbitrary direction of known orientation. We, thus, use the data for D(Mg) parallel to the fastest and slowest diffusion directions (c and b axis, respectively) from Zhang et al. (2010) to calculate the limiting time scales for effectively complete resetting of Mg# in Cpx by shock induced thermal effect. Taking the data for St. Séverin in Figs. 1 and 2 (also Table 1) for the grain radius (~30 μm) and resetting temperature (~870 °C), respectively, we obtain ~10–30 ky for the time scale of resetting of composition of the Cpx grain. If D(Fe–Mg) in Cpx is as slow as the data of Dimanov and Wiedenbeck (2006) suggest, then the resetting time scale is going to increase by a factor 17. However, we feel that such a large increase is unlikely because, as discussed above, use of D (Fe–Mg) data of Dimanov and Wiedenbeck (2006) to model Opx–Cpx profiles in St. Séverin required an unrealistic lowering of D(Fe–Mg) of Ganguly and Tazzoli (1994) by a factor of 300.

The simulations presented by Ciesla et al. (2013: Fig. 7) do not show the duration of post-shock peak temperature that could be compared with the results derived above. Their post-shock T–t paths show very rapid cooling and a transition to very slow cooling at low temperature that have qualitative similarity with the T–t paths constructed in this study (Figs. 3 and 5) and by Ganguly et al. (2013: Fig. 11). However, the transition temperatures in the simulations of Ciesla et al. (2013) (⩽125 °C) are much lower than those deduced from cooling rate studies, which are in the range of 450–500 °C; also these transition temperatures are inconsistent with the slow metallographic cooling rates of chondrites (10–20 °C/My) that are valid at ~550 °C, and thermochronological constraints (Fig 3; Ganguly et al., 2013: Fig. 11) that require initiation of very slow cooling of chondrites (~2 °C/My) at ~500 °C. It remains to be seen if the peak T–t combination derived above as well as the overall two (or more) stage T–t path deduced in this study and Ganguly et al. (1994, 2013) could be generated by impact simulations by varying the model parameters and also considering a wider distribution of samples with respect to the site of impact. Some of the near surface (within 5 km depth) cooling paths generated by Ciesla et al. (2013) are similar to those deduced by Ganguly et al. (2013, Fig. 11) for H4 samples, but it is not clear if the simulated peak thermal conditions are sustained long enough to transform petrologic type 3 to 4. The time needed for this transformation is even greater than that calculated above for the sample from St. Séverin because of lower peak temperature of type 4 chondrites. For example, using the inferred T_o of Forest Vale H-chondrite of ~750 °C (Ganguly et al., 2013), we get 80–560 ky for the transformation of H3 to H4.

3.3. Towards development of a self-consistent model of the internal structure of the asteroidal parent bodies and their impact and thermal histories

It was emphasized by Ganguly et al. (2013) in their study of H chondrites that the rapid cooling rates at high temperature recorded by the pyroxene compositional profiles are not incompatible with an onion-shell parent body model at the initial stage; however, the inferred cooling rates are incompatible with the notion of excavation and delivery of the samples to Earth from their original sites of metamorphism that was caused by internal radiogenic heating of a spherical parent body. Subsequently, Scott et al. (2014) also discussed several contradictions of the age and metal cooling rate data of H-chondrite with the notion of *in situ* cooling in an undisturbed onion-shell parent body. Furthermore, they have shown that the conformity between the onion-shell cooling model of H chondrite and the age data of Trieloff et al. (2003) is a consequence of sampling statistics.

If the asteroidal parent bodies of the meteorites became disrupted by impact, then at least part of the disrupted pieces should be expected to have either gotten (a) accreted to some other asteroidal bodies or (b) buried under ruble piles on the still intact portion of the parent asteroids. As discussed by Ganguly et al. (2013), the scenario (a) predicts that higher metamorphic types (5/6) should be found on the surface of an asteroid, as indeed has been found on the surface of the asteroid Itokawa (Nakamura et al., 2011). The scenario (b) predicts that different metamorphic types should show compositional characteristics of both fast (degrees/ky) and slow (degrees/My) cooling at low temperatures, depending on the post-fragmentation location/burial depth of the samples. Scott et al. (2014) reported both fast (Forest Vale, Beaver Creek, Ste. Marguerite: $\geqslant$50,000 °C/My) and very slow (EET86802, GEO etc.: 4–60 °C/My) metallographic cooling rate for H4 through ~500 °C. The low-T metal cooling rate for Forest Vale is quite similar to its high-T cooling rate deduced from Px-profiles by Ganguly et al. (2013) (also note the possible modification high-T cooling rate in Section 2.3.4). The contrasting cooling rates of H4 differing by several orders of magnitude support the model of fragmentation and burial under rubble pile scenario (model (b)); however, so far low-T cooling rates of higher metamorphic types have been found to be very slow, of the order of 10 °C/My.

Recently Guignard and Toplis (2015) carried out a detailed study of the textural properties of iron-rich phases in H-chondrites and found excellent correlation between average crystal size and the relative depth of the samples that may be inferred on the basis of their metamorphic types and calculated thermal structure in an onion-shell parent body (Monnereau et al., 2013). This observation would be compatible with our suggestion of parent body disruption only if the latter had taken place after the peak thermal conditions were attained at different depths in an onion shell parent body, and no significant grain growth had taken place during subsequent cooling. To test this hypothesis, we have calculated the extent of grain growth using the cooling rates of the samples deduced in this work (Figs. 6–8), and the growth equation in Guignard and Toplis (2015) along with updated kinetic parameters in Guignard et al. (2016), and indeed found practically no additional grain growth during post-shock cooling of the samples. Thus, onion-shell parent body model in which metamorphism took place by internal radiogenic heating may be reconciled with the cooling rates deduced in this study and Ganguly et al. (2013) if it is assumed that the parent bodies suffered disruption after the peak temperatures were attained at different depths, i.e. ~10 Ma after CAI formation.

An alternative model to what has been presented above is to consider two thermal episodes, viz. (i) Impact heating of the samples to high temperatures followed by rapid cooling to the ambient condition, and (ii) a second episode of radiogenic heating and subsequent slow cooling. In order for such a model to be viable, at least two conditions need to be met:

(a) the impact heating must have been sustained for at least 10 ky to set the metamorphic type and the observed compositional homogeneity of minerals, as discussed in the preceding section; and
(b) the T–t path in the stage (ii) must have been such as not to disturb the compositional characteristics of the pyroxenes established during the stage (i).

As remarked above, the available impact simulation study (Ciesla et al., 2013) did not provide adequate data to evaluate if the condition (a) could have been satisfied. With respect to (b), it has been shown, as discussed above, by a number of simulations in this study (Figs. 6 and 8) and in Ganguly et al. (2013) that the transition from rapid high-T cooling rate (~10^2 °C/ky) to four orders of magnitude slower low-T cooling rate that have been constrained by diffusion modeling and metallographic methods, respectively, should have taken place at ~500–550 °C; a higher transition temperature (T(tr)) in the simulations causes disturbance of pyroxene Mg# profiles (see, for example Fig. 8 in which the Mg# profiles were disturbed even at T(tr) = 550 °C). The disturbance would be even more in the scenario of post-impact radioactive heating to this temperature range and subsequent slow cooling since there would be some additional resetting during the prograde limb and peak duration of the T–t path.

The restriction of peak temperature to ~550 °C by radiogenic heating would necessitate a parent body with much lower concentration of heat producing isotopes, especially ^{26}Al, than has been commonly assumed since reducing the size of the parent body to limit T(peak) to ~550 °C may not achieve the slow cooling for H5 and H6 samples deduced from metallographic and thermochronological data. Additionally, we do not see any way to reconcile the textural data of Guignard and Toplis (2015) with such a model.

ACKNOWLEDGMENTS

This research was supported by a NASA grant NNX14AG28G to JG. We are grateful to the curatorial staffs for meteorite collec-

tions of Smithsonian Institution, Johnson Space Center and Arizona State University for lending the meteorite samples used in this study. Constructive reviews by Bruce Watson, Fred Ciesla and an anonymous reviewer have led to substantial improvement of the manuscript. The editorial handling by Mike Toplis that not only involved a thorough and thoughtful review of the manuscript but also discussions through several e-mail exchanges is greatly appreciated.

REFERENCES

Anderson D. J., Lindsley D. H. and Davidson P. M. (1993) QUILF: a Pascal program to assess equilibria among Fe–Mg–Mn–Ti oxides, pyroxenes, olivines and quartz. *Comput. Geosci.* **19**, 1333–1350.

Bevington P. R. and Robinson O. K. (2003) *Data Reduction and Error Analysis for Physical Sciences*. Mc-Graw Hill, 307 p.

Bogard D. D., Garrison D. H., Jordan J. L. and Mittlefehldt D. (1990) ^{39}Ar–^{40}Ar dating of mesosiderites: evidence for major parent body disruption at 4 Ga. *Geochim. Cosmochim. Acta* **54**, 2549–2564.

Bouvier A., Blichert-Toft J., Moynier F., Vervoot J. and Albarede F. (2007) Pb–Pb dating constraints on the accretion and cooling history of chondrites. *Geochim. Cosmochim. Acta* **71**, 1583–1604.

Brey G. P. and Köhler T. (1990) Geothermobarometry in four-phase lherzolites II. New thermobarometers, and practical assessment of existing thermobarometers. *J. Petrol.* **31**, 1353–1378.

Ciesla F. J., Davison T. J., Collins G. S. and O'Brien D. P. (2013) Thermal consequences of impacts in the early solar system. *Meteorit. Planet. Sci.* **48**, 2559–2576.

Crank J. and The Mathematics of Diffusion (1975), second ed. Oxford.

Davison T. M., O'Brien D. P., Ciesla F. J. and Collins G. S. (2013) The early impact histories of meteorite parent bodies. *Meteorit. Planet. Sci.* **48**, 1894–1918.

Dimanov A. and Wiedenbeck M. (2006) (Fe,Mn)–Mg interdiffusion in natural diopside: effect of pO_2. *Eur. J. Mineral.* **18**, 705–718.

Dodson M. H. (1973) Clsoure temperature in cooling geochronological and petrological systems. *Contrib. Mineral. Petrol.* **40**, 259–274.

Ganguly J. (1982) Mg–Fe order-disorder in ferromagnesian silicates II. Thermodynamics, kinetics and geological applications. In *Advances in Physical Geochemistry*, vol. 2 (ed. S. K. Saxena). New York, Springer-Verlag, Berlin, Heidelberg, pp. 58–99.

Ganguly J. and Tazzoli V. (1994) Fe^{2+}–Mg interdiffusion in orthopyroxene: retrieval from the data on intracrystalline exchange reaction. *Am. Mineral.* **79**, 930–937.

Ganguly J. and Tirone M. (1999) Diffusion closure temperature and age of a mineral with arbitrary extent of diffusion. *Earth Planet. Sci. Lett.* **170**, 131–140.

Ganguly J., Bhattacharya R. N. and Chakraborty S. (1988) Convolution effect on the determination of compositional profiles and diffusion coefficients by microprobe step scans. *Am. Mineral.* **73**, 901–909.

Ganguly J., Yang H. and Ghose S. (1994) Thermal history of mesosiderites: quantitative constraints from compositional zoning and Fe–Mg ordering in orthopyroxenes. *Geochim. Cosmochim. Acta* **58**, 2711–2723.

Ganguly J., Tirone M., Chakraborty S. and Domanik K. (2013) H-chondrite parent asteroid: a multi-stage cooling, fragmentation and re-accretion history constrained by thermometric studies, diffusion kinetic modeling and geochronological data. *Geochim. Cosmochim. Acta* **105**, 206–220.

Göpel C., Manhès G. and Allègre C. (1994) U–Pb systematics of phosphates from equilibrated ordinary chondrites. *Earth Planet. Sci. Lett.* **121**, 153–171.

Guignard J. and Toplis M. J. (2015) Textural properties of iron-rich phases in H ordinary chondrites and quantitative links to the degree of thermal metamorphism. *Geochim. Cosmochim. Acta* **149**, 46–63.

Guignard J., Toplis M. J., Bystricky M. and Monnereau M. (2016) Temperature dependent grain growth of forsterite–nickel mixtures: implications for grain growth in two-phase systems and applications to the H-chondrite parent body. *Earth Planet. Sci. Lett.* **443**, 20–31.

Hohenberg C. M., Hudson B., Kennedy B. M. and Podosek F. A. (1981) Noble gas retention chronologies for the St. Séverin meteorite. *Geochim. Cosmochim. Acta* **45**, 535–546.

Kleine T. A., Touboul M., Van Orman J. A., Bourdon M., Maden C., Mezger K. and Halliday A. N. (2008) Hf–W thermochronometry: closure temperatures and constraints on the accretion cooling history of H chondrite parent body. *Earth Planet. Sci. Lett.* **270**, 106–118.

Krot T. A, Goldstein, J. J., Scott E. R. D. and Wakita S. (2012) Thermal histories of H3–H6 chondrites and their parent asteroid from metallographic cooling rates and cloudy taenite dimensions. *Meteoritical Society Meeting* # 5372 (abstr.).

Liermann H.-P. and Ganguly J. (2001) Compositional properties of coexisting orthopyroxene and spinel in some Antarctic diogenites: implications for thermal history. *Meteorit. Planet. Sci.* **36**, 155–166.

Lindsley D. H. (1983) Pyroxene thermometry. *Am. Mineral.* **68**, 477–493.

Min K., Reiners P. W. and Shuster D. L. (2013) (U–Th)/He ages of phosphates from St. Séverin LL6 chondrite. *Geochim. Cosmochim. Acta* **100**, 282–296.

Monnereau M., Toplis M. J., Baratoux D. and Guignard J. (2013) Thermal history of the H-chondrite parent body: implications for metamorphic grade and accretionary time-acales. *Geochim. Cosmochim. Acta* **119**, 302–321.

Müller T., Dohmen R., Becker H.-W., ter Heege J. H. and Chakraborty S. (2013) Fe–Mg interdiffusion rates in clinopyroxene: experimental data and implications for Fe–Mg exchange thermometers. *Contrib. Mineral. Petrol.* **166**, 1563–1576.

Nakamura T., Noguchi T., Tanaka M., Zolensky M. E., Tsuchiyama M. A., Nakato A., Ogami T., Ishida H., Uesugi M., Fujimura A., Okazaki R., Sandford S. A., Ishibashi Y., Abe M., Ueno M., Mukai T., Yoshikawa M. and Kawaguchi J. (2011) Itokawa dust particles: a direct link between S-type aste ordinary chondrites. *Science* **333**, 1113–1116.

O'Neill H. St. C. (1988) Systems Fe–O and Cu–O: thermodynamic data for the equilibria Fe-"FeO", Fe-Fe_3O_4, "FeO"-Fe_3O_4, Cu-Cu_2O from emf measurements. *Am. Mineral.* **73**, 470–486.

Posner E., Ganguly J. and Hervig R. (2016) Diffusion kinetics of Cr in spinel: Experimental studies and implications for ^{53}Mn – ^{53}Cr cosmochronology. *Geochim. Cosmochim. Acta* **175**, 20–35.

Powell B. N. (1969) Petrology and chemistry of mesosiderites I. Textures and compositions of nickel-iron. *Geochim. Cosmochim. Acta* **33**, 789–810.

Prinzhofer A., Papanastassiou D. A. and Wasserburg G. J. (1992) Samarium–neodymium evolution of meteorites. *Geochim. Cosmochim. Acta* **56**, 797–815.

Sano J., Ganguly J., Hervig R. and Dohmen R. (2011) Neodymium diffusion in orthopyroxene: experimental study problemies and applications to geological and planetary problems. *Geochim. Cosmochim. Acta* **75**, 4684–4698.

Scott E. R. D., Krot T. V., Goldstein J. I. and Wakita S. (2014) Thermal and impact history of H chondrite parent asteroid during metamorphism: constraints from metallic Fe–Ni. *Geochim. Cosmochim. Acta* **136**, 13–37.

Trieloff M., Jesserberger E. K., Herrwerth I., Hopp J., Fiénel C., Ghélls M., Bourot-Denise M. and Pellas P. (2003) Structure and thermal history of H-chondrite parent asteroid revealed by thermochronometry. *Nature* **422**, 502–506.

van Niekerk D., Scott E. R. D. and Taylor J. (2014) Constraints on the thermal and impact history of ordinary chondrites from two-pyroxene equilibration temperatures. *48th Lunar Planet. Sci. Conf.* #2374 (abstr.).

Wasson J. T. and Wang S. (1991) The histories of ordinary chondrite parent bodies. U, Th–He age distributions. *Meteoritics* **26**, 161–167.

Wood J. A. (1967) Chondrites: their metallic minerals, thermal histories and parent planets. *Icarus* **6**, 1–49.

Zhang X., Ganguly J. and Ito M. (2010) Ca–Mg diffusion in diopside: tracer and chemical inter-diffusion coefficients. *Contrib. Mineral. Petrol.* **150**, 175–186.

Associate editor: Michael J. Toplis